Journal of Cosmology and Astroparticle Physics
An IOP and SISSA journal

Scalar correlation functions for a double-well potential in de Sitter space

Tommi Markkanen[a,b] **and Arttu Rajantie**[c]

[a]Laboratory of High Energy and Computational Physics,
National Institute of Chemical Physics and Biophysics,
Rävala pst. 10, Tallinn, 10143, Estonia
[b]Helsinki Institute of Physics,
P.O. Box 64, FIN-00014 University of Helsinki, Finland
[c]Department of Physics, Imperial College London,
London, SW7 2AZ, United Kingdom

E-mail: tommi.markkanen@kbfi.ee, a.rajantie@imperial.ac.uk

Received January 31, 2020
Accepted February 19, 2020
Published March 24, 2020

Abstract. We use the spectral representation of the stochastic Starobinsky-Yokoyama approach to compute correlation functions in de Sitter space for a scalar field with a symmetric or asymmetric double-well potential. The terms in the spectral expansion are determined by the eigenvalues and eigenfunctions of the time-independent Fokker-Planck differential operator, and we solve them numerically. The long-distance asymptotic behaviour is given by the lowest state in the spectrum, but we demonstrate that the magnitude of the coeffients of different terms can be very different, and the correlator can be dominated by different terms at different distances. This can give rise to potentially observable cosmological signatures. In many cases the dominant states in the expansion do not correspond to small fluctuations around a minimum of the potential and are therefore not visible in perturbation theory. We discuss the physical interpretation these states, which can be present even when the potential has only one minimum.

Keywords: physics of the early universe, quantum field theory on curved space

ArXiv ePrint: 2001.04494

© 2020 IOP Publishing Ltd and Sissa Medialab https://doi.org/10.1088/1475-7516/2020/03/049

JCAP03(2020)049

Contents

1 Introduction

The study of a quantized scalar field in de Sitter space is a mature endeavour [1–4] possessing well-known difficulties when the field is light [5–8]. Light spectator scalars in de Sitter space are not just of formal interest, but rather they can have a variety of cosmological implications such as generation of dark matter [9–11] or triggering electroweak vacuum decay [12–14]. The stochastic approach presented in refs. [15, 16] is a powerful way of addressing this problem; it is analytically tractable yet it provides accurate results that are often superior to more traditional resummation methods. The approach is based on the realization that the ultraviolet part of the field may to a good approximation be treated as white noise allowing one to express all results via classical stochastics. For other techniques, see refs. [17–29]

The stochastic approach has become increasingly popular in recent years, likely due to its great efficacy, and in this vein we note the recent works [30–46]. Often the focus is on the local probability distribution of the field or on local expectation values, even though the correlation of fluctutations over space is arguably the more relevant object physically. The spatial correlators have been addressed for example in refs. [9, 11, 35, 47–59]. Specifically, in ref. [59] it was shown how correlators at noncoincident points can be effectively calculated with numerical techniques in conjunction with the spectral expansion based on eigenfunctions and -values already discussed in ref. [15].

The focus of ref. [59] was on a single spectator scalar ϕ with quadratic and quartic terms in its potential while limiting the parameters to only include positive mass terms i.e.

JCAP03(2020)049

potentials possessing a single minimum at the origin. In this work we extend this analysis to include potentials with two possibly non-degenerate minima. Namely, we focus on a potential of the form

$$V(\phi) = \mu^3\phi + \frac{1}{2}m^2\phi^2 + \frac{\lambda}{4}\phi^4\,, \tag{1.1}$$

with $m^2 \leq 0$ and $\mu \geq 0$. Throughout we will make use of the parametrization[1]

$$\bar{\alpha} \equiv \frac{-m^2}{\sqrt{\lambda}H^2}\,; \quad \beta \equiv \frac{\mu^3}{\lambda^{1/4}H^3}\,; \quad \bar{m}^2 \equiv -m^2\,. \tag{1.2}$$

This potential has two minima if $\bar{\alpha} > 3(\beta/2)^{2/3}$. In typical perturbative treatments, the field is assumed to fluctuate near the minimum of the potential, but the stochastic spectral expansion does not require that assumption. As we will show, in many cases the dominant contributions to the correlators come from large-amplitude fluctuations that are not visible in perturbation theory.

This paper is organised as follows: in section 2 we summarise the stochastic spectral expansion and the numerical technique we used to find the terms in the expansion. In sections 3 and 4, we apply these techniques to calculate the spectral expansion in the symmetric and asymmetric cases, respectively. In section 5 we discuss the physical interpretation and implications of our results, and in section 6 we summarise our conclusions.

2 The stochastic spectral expansion

2.1 The eigenvalue equation

In the stochastic formalism one may express any correlator involving noncoincident spacetime points as a spectral expansion [16, 59], by solving the eigenvalues and eigenfunctions, Λ_n and ψ_n, from the eigenvalue equation

$$D_\phi\psi_n = -\frac{4\pi^2\Lambda_n}{H^3}\psi_n\,, \tag{2.1}$$

with

$$D_\phi = \frac{1}{2}\frac{\partial^2}{\partial\phi^2} - \frac{1}{2}W(\phi)\,; \quad v(\phi) = \frac{4\pi^2}{3H^4}V(\phi)\,; \quad W(\phi) = v'(\phi)^2 - v''(\phi)\,. \tag{2.2}$$

Since the input in the eigenvalue equation (2.1) is $W(\phi)$ (and not $V(\phi)$) it is the $W(\phi)$ that will turn out to be the fundamental quantity providing a qualitative understanding of the behaviour of the eigenfunctions and -values. The behavior of $v(\phi)$ and $W(\phi)$ for the potential (1.1) is illustrated in figure 1. In most cases solving equation (2.1) needs numerical methods.

2.2 Correlators and the power spectrum

If $G_f(t_2, t_1; \mathbf{x}_2, \mathbf{x}_1)$ is the general correlator for some function of the field $f(\phi)$, the autocorrelation function

$$G_f(t; 0) = \langle f(\phi(0))f(\phi(t))\rangle, \tag{2.3}$$

[1] This is related to the definition in ref. [59] as $\bar{\alpha} \equiv -\alpha$.

JCAP03(2020)049

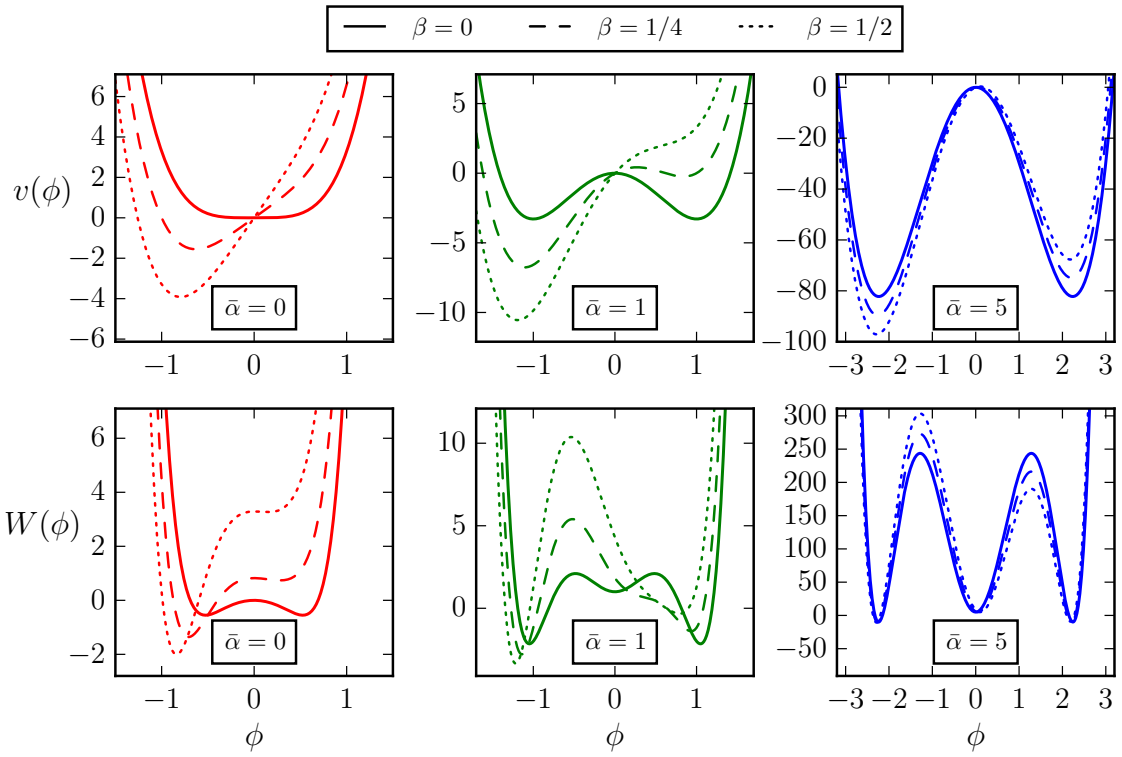

Figure 1. The $v(\phi)$ and $W(\phi)$ potentials as defined in (2.2) with the choice $\lambda = 1$ given in the units $H = 1$.

can via the stochastic formalism be expressed as a spectral expansion [16, 59] making use of the eigenfunctions and -values from eq. (2.1). Specifically, in terms of eigenvalues Λ_n and spectral coefficients f_n one may write

$$G_f(t;0) = \sum_n f_n^2 e^{-\Lambda_n t}\,, \tag{2.4}$$

where the spectral coefficients are specific to the form of $f(\phi)$

$$f_n \equiv \int d\phi \psi_0 f(\phi) \psi_n\,. \tag{2.5}$$

By making use of the de Sitter invariance of the equilibrium quantum state, from (2.4) one may infer the form of the equal time correlator between two spatially separated points

$$G_f(0;\mathbf{x}) = \sum_n \frac{f_n^2}{(|\mathbf{x}|H)^{2\Lambda_n/H}}\,, \tag{2.6}$$

where $\mathbf{x}$ is physical.

2.3 A numerical approach

Following we solve the eigenfunctions and eigenvalues of eq. (2.1) numerically with the 'overshoot/undershoot' or otherwise known as 'wag the dog' method. For a potential with $\mathbb{Z}_2$

JCAP03(2020)049

symmetry this problem reduces to a systematic iteration of just one unknown variable, the eigenvalue Λ_n. This is due to the general feature that for a symmetric potential the wave functions are either even or odd, which fixes one of the two initial conditions required for a second order differential equation and the remaining one is irrelevant as the functions must be normalized. The essentials of the method are well-known and can be found for example in section 2.3 of ref. [60]. This special case is encoutered in the symmetric double-well potential, which is addressed in section 3. A major shortcoming is that modifications are required when two eigenvalues are (almost) degenerate, which is encountered at the limit of a large barrier, or equivalently, deep wells. However as we will show, this is precisely the limit for which one may easily derive accurate analytic approximations and with a combination of analytics an numerics the entire eigenvalue spectrum may be covered.

When there is no $\mathbb{Z}_2$ symmetry, for example as in eq. (1.1) with $\beta \neq 0$ that is discussed in section 4, the 'overshoot/undershoot' needs to be performed with respect to two unknowns: in addition to the eigenvalue one must iterate over the value or derivative of the function at a point giving rise to a two dimensional iteration problem. This however amounts to only a small increase in complexity of the algorithm or the expensiveness of the computation.

To facilitate a numerical analysis of the eigenfunctions and -values very similarly to ref. [59] for the potential (1.1) it is convenient to introduce the following dimensionless quantities

$$z \equiv \frac{\lambda^{1/4}\Omega}{H}\phi, \qquad \Omega \equiv \left(1 + \frac{\bar{m}}{H\lambda^{1/4}} + \frac{\mu^3}{\lambda^{1/4}H^3}\right) \equiv \left(1 + \sqrt{\bar{\alpha}} + \beta\right), \tag{2.7}$$

$$\tilde{\Lambda}_n \equiv \frac{\Lambda_n}{\lambda^{1/2}H + \bar{m}^2/H + \mu^6/H^5} \equiv \frac{\Lambda_n}{\lambda^{1/2}H(1 + \bar{\alpha} + \beta^2)}, \tag{2.8}$$

so that the eigenvalue equation (2.1) may be written in terms of dimensionless numbers as

$$\left\{\frac{\partial^2}{\partial z^2} - 4\pi^2\frac{\bar{\alpha} + \frac{4\pi^2}{3}\beta^2}{3\Omega^2} + \frac{32\pi^4\bar{\alpha}\beta z}{9\Omega^3} + 4\pi^2\frac{1 - \frac{4\pi^2}{9}\bar{\alpha}^2}{\Omega^4}z^2 - \frac{32\pi^4\beta z^3}{9\Omega^5} + \frac{32\pi^4\bar{\alpha}z^4}{9\Omega^6} - \frac{16\pi^4 z^6}{9\Omega^8} + \frac{8\pi^2\left(1 + \bar{\alpha} + \beta^2\right)\tilde{\Lambda}_n}{\Omega^2}\right\}\psi_n = 0, \tag{2.9}$$

with the $\bar{\alpha}$ and β given in (1.2). Furthermore and precisely as in ref. [59] we also introduce scaled eigenfunctions

$$\psi_n \equiv \sqrt{\frac{\lambda^{1/4}\Omega}{H}}\tilde{\psi}_n \quad \Rightarrow \quad \int_{-\infty}^{\infty} d\phi\, |\psi_n|^2 = \int_{-\infty}^{\infty} dz\, |\tilde{\psi}_n|^2 = 1\,. \tag{2.10}$$

There are two reasons why the redefinitions we introduced are very useful for numerical work. First, as one can see from eq. (2.9), unlike the potential that is a function of μ, m and λ there are only two unknown parameters, $\bar{\alpha}$ and β. Second, there are no terms in the equation that would grow without bound at any of the limiting cases $\bar{\alpha} \to 0$, $\bar{\alpha} \to \infty$, $\beta \to 0$ and $\beta \to \infty$, so broadly speaking all numerical factors are of the same order throughout the parameter space of interest.

3 The symmetric double-well potential

3.1 The first five eigenfunctions/-values

Before addressing the general situation, let us first focus on the important special case of a symmetric double-well potential with two degenerate minima i.e. with $\beta = 0$. The first four

JCAP03(2020)049

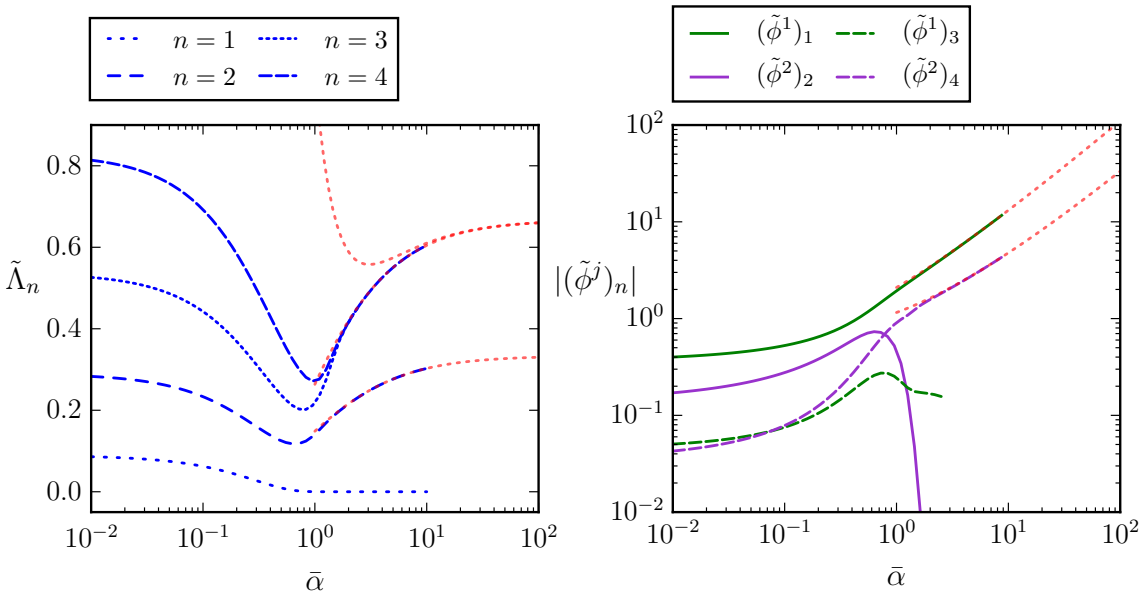

Figure 2. The lowest eigenvalues (left) and spectral coefficients for $f(\phi) = \phi$ and $f(\phi) = \phi^2$ (right) in the symmetric case, $\beta = 0$. The red dotted lines show the analytic approximations (3.9), (3.10), (3.11), (3.13) and (3.14).

non-trivial eigenvalues are plotted in figure 2. For $\bar{\alpha} \gtrsim 2.5$ the eigenvalues Λ_3 and Λ_4 become degenerate, complicating the numerical analysis, but by this point analytic approximations derived in section 3.2 (depicted with red dotted lines) are already very accurate.

The eigenfunctions $\tilde{\psi}_n$ for $n \leq 4$ are shown in figure 3. For $\bar{\alpha} \gtrsim 1$ the system separates into linear combinations of solutions centered at the three minima of $W(\phi)$, which can be seen in figure 1. Importantly, there are solutions that do not vanish close to the origin, even when $\bar{\alpha} \gg 1$ which corresponds to a double-well potential with a very large barrier. The clearest example of this is $\tilde{\psi}_2$ at $\bar{\alpha} = 2.5$, which is localised around the top of the potential barrier. As discussed in section 5, these solutions can be interpreted as a contribution from transitions between the two minima, during which the field can spend a significant amount of time near the top of the barrier. The existence of such solutions was apparently not noticed in ref. [16].

3.2 The large barrier limit

As can be seen from figure 1, in the limit a large $\bar{\alpha}$ the potential $W(\phi)$ in the eigenvalue equation (2.1) will possess three minima separated by large barriers, which can be shown to occur at

$$z_0 = 0\,; \qquad z_\pm = \pm\frac{\sqrt{\bar{\alpha}}+1}{\sqrt{3}}\left(\sqrt{\bar{\alpha}^2 + \frac{27}{4\pi^2}} + 2\bar{\alpha}\right)^{1/2}. \tag{3.1}$$

Hence, at the limit $\bar{\alpha} \to \infty$, the system separates into three quadratic pieces, which can be obtained from (2.9) by expanding around a large $\bar{\alpha}$ with $\beta = 0$.

JCAP03(2020)049

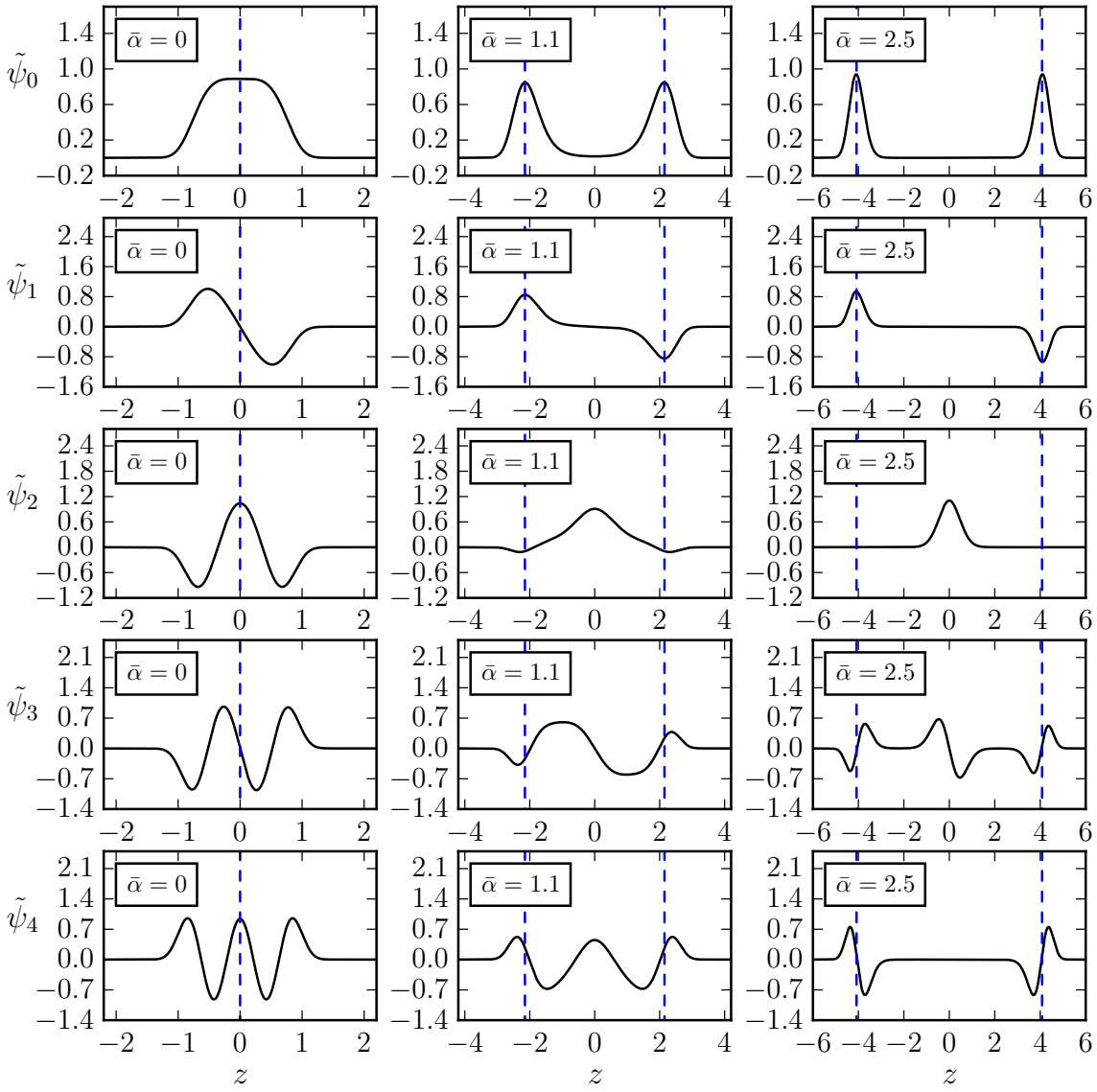

Figure 3. The dimensionless eigenfunctions $\tilde{\psi}_n$ from eq. (2.10) for the symmetric potential (1.1) with $\beta = 0$ as a function of $\bar{\alpha} \equiv \bar{m}^2/(H^2\sqrt{\lambda})$ The blue dashed lines indicate the locations of the minima of the potential $V(\phi)$.

For completeness[2] we first write the eigenvalue equation for $V(\phi) = \frac{1}{2}M^2\phi^2$

$$\left\{\frac{\partial^2}{\partial x^2} - \left(\frac{4\pi^2}{3}\right)^2 x^2 + \frac{4\pi^2}{3} + 8\pi^2\tilde{\Lambda}_n\right\}\psi_n = 0\,; \quad x = \frac{M}{H^2}\phi\,; \quad \tilde{\Lambda}_n = \frac{\Lambda_n}{M^2/H}\,, \tag{3.2}$$

with the eigenfunctions and -values

$$\psi_n = \frac{\sqrt{M}}{H}\frac{1}{\sqrt{2^n n!}}\left(\frac{4\pi}{3}\right)^{1/4} e^{-\frac{2\pi^2x^2}{3}} H_n\left(\frac{2\pi x}{\sqrt{3}}\right)\,; \quad \Lambda_n = \frac{n}{3}\frac{M^2}{H}\,. \tag{3.3}$$

[2]See ref. [59] for more discussion and plots.

JCAP03(2020)049

Close to the origin at the limit of large barriers i.e. taking $\bar{\alpha} \to \infty$ we then get the approximate eigenvalue equation for the potential (1.1)

$$\left\{\frac{\partial^2}{\partial z^2} - \left(\frac{4\pi^2}{3}\right)^2 z^2 + \frac{4\pi^2}{3} + 8\pi^2\left(\tilde{\Lambda}_n - \frac{1}{3}\right)\right\}\psi_n^0 = 0\,; \quad z = \frac{\bar{m}}{H^2}\phi\,; \quad \tilde{\Lambda}_n = \frac{\Lambda_n}{\bar{m}^2/H}\,, \tag{3.4}$$

where the eigenfunctions and -values can be read off from the quadratic results (3.3)

$$\psi_n^0 = \frac{\sqrt{\bar{m}}}{H}\frac{1}{\sqrt{2^n n!}}\left(\frac{4\pi}{3}\right)^{1/4} e^{-\frac{2\pi^2 z^2}{3}} H_n\left(\frac{2\pi z}{\sqrt{3}}\right)\,; \quad \Lambda_n = \frac{n+1}{3}\frac{\bar{m}^2}{H}\,. \tag{3.5}$$

At $z_\pm$ for large barriers one gets the approximate equation

$$\left\{\frac{\partial^2}{\partial y^2} - \left(\frac{4\pi^2}{3}\right)^2 y^2 + \frac{4\pi^2}{3} + 8\pi^2\left(\frac{\tilde{\Lambda}_n}{2}\right)\right\}\psi_n^\pm = 0\,; \quad y = \sqrt{2}(z - z_\pm)\,; \quad \tilde{\Lambda}_n = \frac{\Lambda_n}{\bar{m}^2/H}\,, \tag{3.6}$$

with the eigenfunctions and -values

$$\psi_n^\pm = \frac{\sqrt{\bar{m}}}{H}\frac{1}{\sqrt{2^n n!}}\left(\frac{8\pi}{3}\right)^{1/4} e^{-\frac{2\pi^2 y^2}{3}} H_n\left(\frac{2\pi y}{\sqrt{3}}\right)\,; \quad \Lambda_n = \frac{2n}{3}\frac{\bar{m}^2}{H}\,. \tag{3.7}$$

By making use of the approximate solutions close to the origin and/or $z_\pm$, (3.5) and (3.7) respectively, and using figure 3 as a guide is it possible to understand qualitatively the large $\bar{\alpha}$ behaviour and often write analytic approximations for the eigenfunctions and -values.

Suppose an analytic function $\Phi_n(\phi)$ that approximates the full solution. Then, by calculating the expectation value of the eigenvalue equation (2.1) one gets an approximation for the eigenvalue as

$$\int d\phi\, \Phi_n D_\phi \Phi_n \approx -\frac{4\pi^2 \Lambda_n}{H^3}\,. \tag{3.8}$$

For example, from figure 3 we see that for large $\bar{\alpha}$ the $n = 1$ eigenfunction approaches an antisymmetric combination of two quadratic $n = 0$ solutions centered at $z_\pm$ (3.7). The eigenvalues of the quadratic $n = 0$ solutions are zero at $z_\pm$ as given by (3.7), which implies that the first exited state has a neglibigle eigenvalue at this limit. As derived in [16], for any large but finite $\bar{\alpha}$ the $n = 1$ eigenvalue is exponentially small.

Similarly, we see that the eigenfunction for $n = 2$ approaches the quadratic $n = 0$ solution at the origin, which as (3.5) shows does not result in a vanishing eigenvalue, even at $\bar{\alpha} \gg 1$. The analytic estimate for the eigenvalue is obtained by

$$\begin{aligned} &\int d\phi\, \psi_0^0 D_\phi \psi_0^0 \approx -\frac{4\pi^2 \Lambda_2}{H^3} \\ &\quad \Rightarrow \quad \tilde{\Lambda}_2 \approx \frac{32\pi^2\left(8\pi^2\bar{\alpha}^2 - 9\right)\bar{\alpha}^2 + 135}{768\pi^4\bar{\alpha}^3(\bar{\alpha}+1)} = \frac{1}{3}\left(1 - \frac{1}{\bar{\alpha}} + \frac{1 - \frac{9}{8\pi^2}}{\bar{\alpha}^2}\right) + \mathcal{O}(\bar{\alpha}^{-3})\,. \end{aligned} \tag{3.9}$$

The $n = 3$ case can be seen from figure 3 to approach a linear combination of three quadratic $n = 1$ solutions centered at the origin and at $z_\pm$. From (3.5) and (3.7) we see that the solutions are degenerate so we can derive an analytic approximation for the eigenvalue by simply using only the solution at z_0 giving

$$\begin{aligned} &\int d\phi\, \psi_1^0 D_\phi \psi_1^0 \approx -\frac{4\pi^2 \Lambda_3}{H^3} \\ &\quad \Rightarrow \quad \tilde{\Lambda}_3 \approx \frac{512\pi^4\bar{\alpha}^4 - 1152\pi^2\bar{\alpha}^2 + 945}{768\pi^4\bar{\alpha}^3(\bar{\alpha}+1)} = \frac{2}{3}\left(1 - \frac{1}{\bar{\alpha}} + \frac{1 - \frac{9}{4\pi^2}}{\bar{\alpha}^2}\right) + \mathcal{O}(\bar{\alpha}^{-3})\,. \end{aligned} \tag{3.10}$$

JCAP03(2020)049

Finally, the $n = 4$ eigenfunction clearly approaches a symmetric combination of two quadratic $n = 1$ solutions centered at $z_\pm$, with then the eigenvalue at the large $\bar{\alpha}$ limit approximated by

$$\int d\phi\, \psi_1^\pm D_\phi \psi_1^\pm \approx -\frac{4\pi^2 \Lambda_4}{H^3} \quad \Rightarrow \quad \tilde{\Lambda}_4 \approx \frac{2}{3}\left(1 - \frac{1}{\bar{\alpha}} + \frac{1 + \frac{1341}{256\pi^2}}{\bar{\alpha}^2}\right) + \mathcal{O}(\bar{\alpha}^{-3})\,. \tag{3.11}$$

In the above for $n = 4$ we have only included the leading terms as the full result is quite complicated.

The analytic approximations of this section are depicted by the red dashed curves in the left panel in figure 2. As one may see, they are in very good agreement with the full results for $\bar{\alpha} \gtrsim 1$.

3.3 The spectral coefficients

In addition to the eigenvalues, the spectral coefficients are the other ingredient needed for calculating correlators as given by eq. (2.4) and (2.6). As an illustration in the following we analyse the leading and next-to-leading spectral coefficients for $f(\phi) = \phi$ and $f(\phi) = \phi^2$. A useful dimensionless definition comes via (see eq. (2.10))

$$(\tilde{\phi}^j)_n \equiv \left(\frac{\lambda^{1/4}\Omega}{H}\right)^j (\phi^j)_n = \left(\frac{\lambda^{1/4}\Omega}{H}\right)^j \int_{-\infty}^{\infty} d\phi \psi_0 \phi^j \psi_n = \int_{-\infty}^{\infty} dz\, \tilde{\psi}_0 z^j \tilde{\psi}_n\,. \tag{3.12}$$

Much like for the eigenvalues, the spectral coefficients can in some circumstances be approximated with analytic results at the large barrier limit, which may be deduced from section 3.2 and in particular figure 3.

Let us focus on $f(\phi) = \phi$ first. Because it is an odd function, only odd n contribute. Because the ground state and the first exited state approach symmetric and antisymmetric combinations of the ground state of a harmonic oscillator located at $z_\pm$, we may approximate the $(\phi^1)_1$ coefficient as

$$\begin{aligned} |(\phi^1)_1| &\approx \Big| \int_{-\infty}^{\infty} d\phi \frac{1}{\sqrt{2}} \left(\psi_0^+ + \psi_0^-\right) \phi \frac{1}{\sqrt{2}} \left(\psi_0^- - \psi_0^+\right) \Big| \approx \Big| \int d\phi\phi \left(\psi_0^\pm\right)^2 \Big| \\ \Rightarrow \quad |(\tilde{\phi}^1)_1| &\approx \Big| \int dz z \left(\tilde{\psi}_0^\pm\right)^2 \Big| = \frac{\left(\sqrt{\bar{\alpha}} + 1\right)\sqrt{\sqrt{4\pi^2\bar{\alpha}^2 + 27} + 4\pi\bar{\alpha}}}{\sqrt{6\pi}}\,. \end{aligned} \tag{3.13}$$

The third excited state is for large $\bar{\alpha}$ approximately a linear combination of ψ_1^0 and $-\psi_1^+ - \psi_1^-$. For this case in our approximative prescription there is an ambiguity as there is no a priori way to determine the relative size between ψ_1^0 and $-\psi_1^+ - \psi_1^-$.

The analytic approximations (3.13) and (3.14), as well as the numerical results for the leading and next-to-leading spectral coefficients are shown in figure 2. The $|(\tilde{\phi}^1)_3|$ term, shown by the dashed green line, is cut short by our inability to extend the numerical method to cases with almost degenerate eigenvalues, which occurs for $n = 3$. However, it is clearly subleading to $|(\tilde{\phi}^1)_1|$ denoted with green that does not suffer from this issue.

Correspondingly, because $f(\phi) = \phi^2$ is even, only even values of n contribute to its correlator. Since there is virtually no overlap with the $n = 0$ and $n = 2$ solutions at the large barrier limit, $|(\tilde{\phi}^2)_2|$ is expected to vanish up to exponentially small terms. In contrast, $(\phi^2)_4$

JCAP03(2020)049

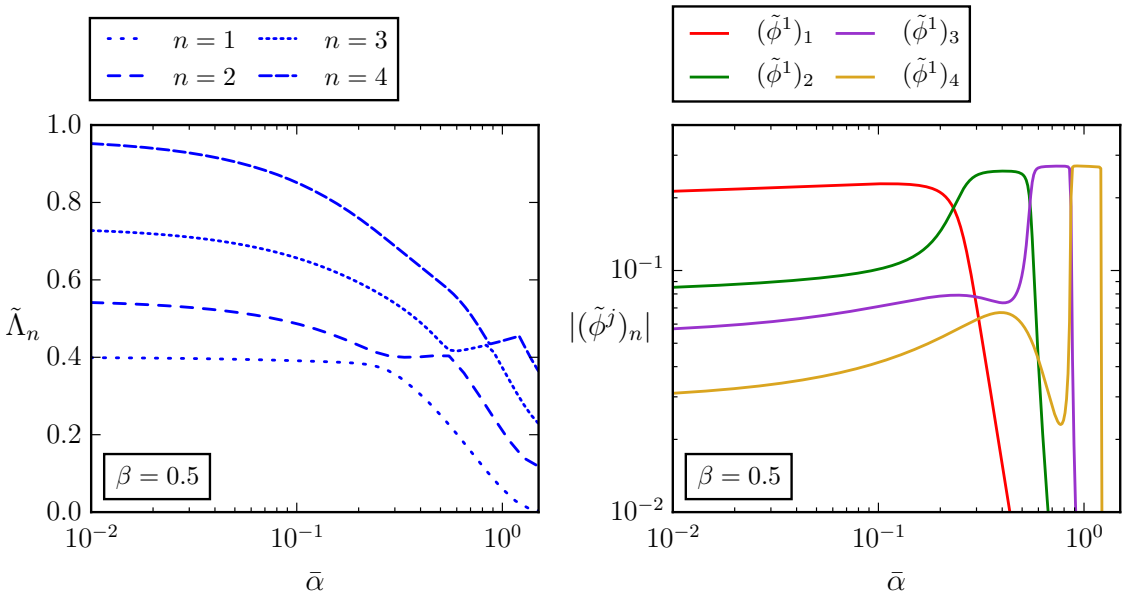

Figure 4. The eigenvalues $\tilde{\Lambda}_n$ (left) and the spectral coefficients for $f(\phi) = \phi$ (right) in the asymmetric case with $\beta = 0.5$, as functions of $\bar{\alpha}$.

has the approximation

$$|(\phi^2)_4| \approx |\int_{-\infty}^{\infty} d\phi \frac{1}{\sqrt{2}} \left(\psi_0^+ + \psi_0^-\right) \phi^2 \frac{1}{\sqrt{2}} \left(\psi_1^+ - \psi_1^-\right)| \approx |\int d\phi \phi^2 \psi_0^\pm \psi_1^\pm|$$

$$\Rightarrow \quad |(\tilde{\phi}^2)_4| \approx |\int dz z^2 \tilde{\psi}_0^\pm \tilde{\psi}_1^\pm| = \frac{\left(\sqrt{\bar{\alpha}} + 1\right)^2 \sqrt{8\pi + \frac{2\sqrt{4\pi^2\bar{\alpha}^2 + 27}}{\bar{\alpha}}}}{4\pi^{3/2}} \,. \tag{3.14}$$

This, together with the numerical results for $|(\tilde{\phi}^2)_2|$ and $|(\tilde{\phi}^2)_4|$ are shown in figure 2 . The fact that $|(\phi^2)_4|$ can dominate over $|(\phi^2)_2|$ as seen in figure 2 has important physical consequences, which are discussed in section 5.

4 The asymmetric double-well potential

Let us now move to the more general asymmetric case, with $\beta > 0$. Now, the potential $V(\phi)$ has a single minimum if $\bar{\alpha} < 3(\beta/2)^{2/3}$, and two non-degenerate minima if $\bar{\alpha} > 3(\beta/2)^{2/3}$. On the hand, the function $W(\phi)$, which appears in the eigenvalue equation (2.1), seems to always have several minima. Depending on its specific form, some of the lowest eigenfunctions may be localised at the other minima of $W(\phi)$, rather than the vacuum state located at the minimum of the potential $V(\phi)$. These contributions would not be visible in typical perturbation theory calculations. They can also give rise to non-trivial hierarchies between the spectral coefficients (2.5).

As an illustrative example, figure 4 shows the lowest eigenvalues for $\beta = 0.5$ as well as the corresponding spectral coeffients for $f(\phi) = \phi$. At $\bar{\alpha} = 0$, the lowest eigenvalue Λ_1 is localised around the vacuum state and therefore it corresponds to perturbative fluctuations. However, when $\bar{\alpha}$ becomes larger, it is overtaken by other eigenvalues which are localised around the other minima of $W(\phi)$.

JCAP03(2020)049

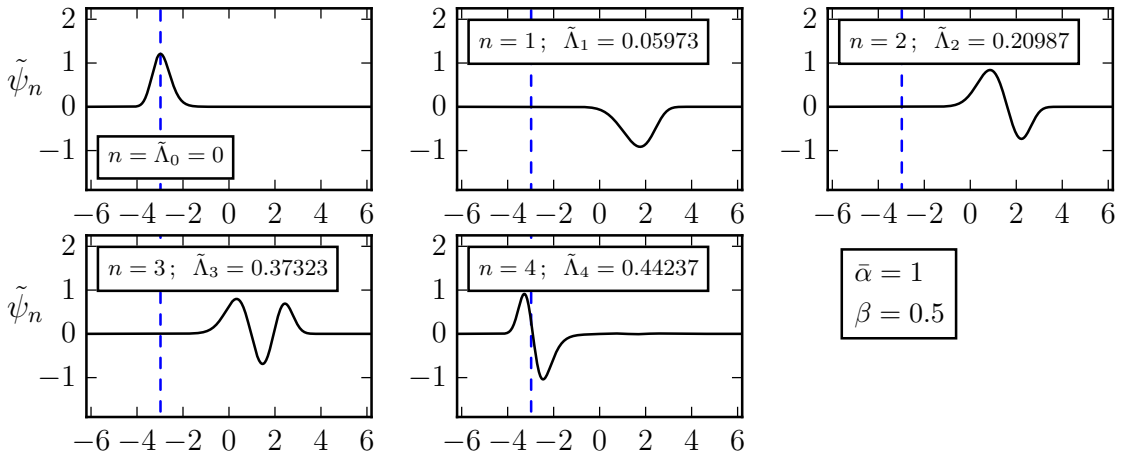

Figure 5. The $n \leq 4$ eigenfunctions and their respective eigenvalues from (2.9) with $\bar{\alpha} = 1$ and $\beta = 0.5$. The blue dashed line indicates the location of the minimum of the potential.

This can be seen in figure 5, which shows the five lowest eigenfunctions for $\bar{\alpha} = 1$ and $\beta = 0.5$. Even though the potential $V(\phi)$ actually has only one minimum for these parameters (see figure 1), the lowest excited state localised at the minimum of the potential is $n = 4$. The asymptotic form of the correlator is therefore determined by the shape of the potential away from its minimum. However, because such states have a very small overlap with the ground state ψ_0, their spectral coefficients are very small. This is discussed more in section 5. The eigenfunctions and -values up to $n = 4$ for some representative choices for $\bar{\alpha}$ and β are shown in figures 8–12 in appendix A.

5 Discussion

5.1 Length scales

In cosmology, the observable length scales correspond to comoving distances that were many orders of magnitude longer than the Hubble length during inflation. We are therefore often interested in the correlator at distances that are very long but still finite.

The asymptotic long-distance behaviour of the correlator $G_f(0, r)$ is given by the first term in the spectral expansion (2.6) with a non-zero spectral coefficient f_n. The behaviour is simplest if the lowest state, $n = 1$, has the largest spectral coefficient, because then the correlator is well approximated by a single power-law at all length scales,

$$G_f(0, r) \approx \frac{f_1^2}{(rH)^{2\Lambda_1/H}}. \tag{5.1}$$

However, this is not always the case, and more generally, the correlator can be dominated by a higher term $n = d$ in the expansion at the distances of interest,

$$G_f(0, r) \approx \frac{f_d^2}{(rH)^{2\Lambda_d/H}}. \tag{5.2}$$

In particular, the short-distance behaviour of the correlator can be very different from its asymptotic long-distance form. To characterise that, following ref. [16] we define a correlation

JCAP03(2020)049

radius to be the distance where the correlator has fallen to half of its value at $r = 1/H$,

$$G_f(0, R_f) = \frac{1}{2} G_f(0, 1/H) \,. \tag{5.3}$$

When a single coefficient $n = d$ dominates the correlator, this simply gives

$$R_f \approx H^{-1} 2^{\frac{H}{2\Lambda_d}} \,. \tag{5.4}$$

The non-trivial hierarchies between different terms in the spectral expansion can be important for cosmological observations. If there is a change in the behaviour of the correlator within the observable scales, it can potentially be detected providing useful information about the fields responsible for it.

5.2 Symmetric potential

In the symmetric case ($\beta = 0$) discussed in section 3, there are two examples of this non-trivial behaviour. The first is that, because the lowest eigenstate $n = 1$ has odd parity, the corresponding spectral coefficient vanishes for all even functions. The asymptotic long-distance behaviour of any even correlator, such as those of ϕ^2 or the energy density, is therefore given by the second-lowest eigenvalue Λ_2. When $\bar{\alpha} \gtrsim 1$, the difference between them can be large, as we can see from the left panel in figure 2. Because Λ_1 is small, the field itself is correlated over massively superhorizon scales, but its energy density is not, because its correlations are determined by Λ_2. The physical reason for this behaviour is that on superhorizon scales, the system consists of domains of the two vacua, which contribute to the field correlator, and the correlation radius R_ϕ gives the typical size of these domains. However, because both vacua have the same energy density, these domains do not give any contribution to correlators of even quantities such as the energy density.

The second example is that, as we can see from the right panel of figure 2, the spectral coefficient of ϕ^2 for the second-lowest state $n = 2$ falls rapidly when $\bar{\alpha} \gtrsim 1$. This means that although the asymptotic long-distance behaviour of any even correlator is indeed given by Λ_2, it only starts to dominate at very long superhorizon distances, and at shorter distances the dominant contribution is given by Λ_4. To understand why this happens, it is useful to look at the corresponding eigenfunctions in figure 3. The higher state ψ_4 is localised at the minima of the potential, and therefore it corresponds to small-amplitude perturbative fluctuations around either vacuum state. The lower state ψ_2, on the other hand, is localised on top of the barrier, $\phi = 0$, which shows that this contribution comes from the boundaries between the domains. The eigenvalue Λ_2 characterises the thickness of these domain walls, and the spectral coefficient is small because their volume is small compared with the volume of the domains.

The different behaviour of odd and even correlators is illustrated by figure 6, which shows the correlation radii of ϕ and $\delta\phi^2$. As Λ_1 becomes small, the field correlation radius grows to massively superhorizon scales. In contrast, when $\bar{\alpha} \gtrsim 1$, the correlation radius of $\delta\phi^2$ starts to decrease, first because Λ_2 grows, and then because Λ_4 starts to dominate it.

If any variable has significant correlations at distances much longer than the current Hubble length $1/H_0$, they would appear as a homogeneous background value. In the case of a symmetric potential, this happens when the domain size is larger than $1/H_0$, in which case the current observable Universe would most likely be inside single domain. In that case the observed field correlator would be determined by the second-lowest odd eigenvalue Λ_3.

JCAP03(2020)049

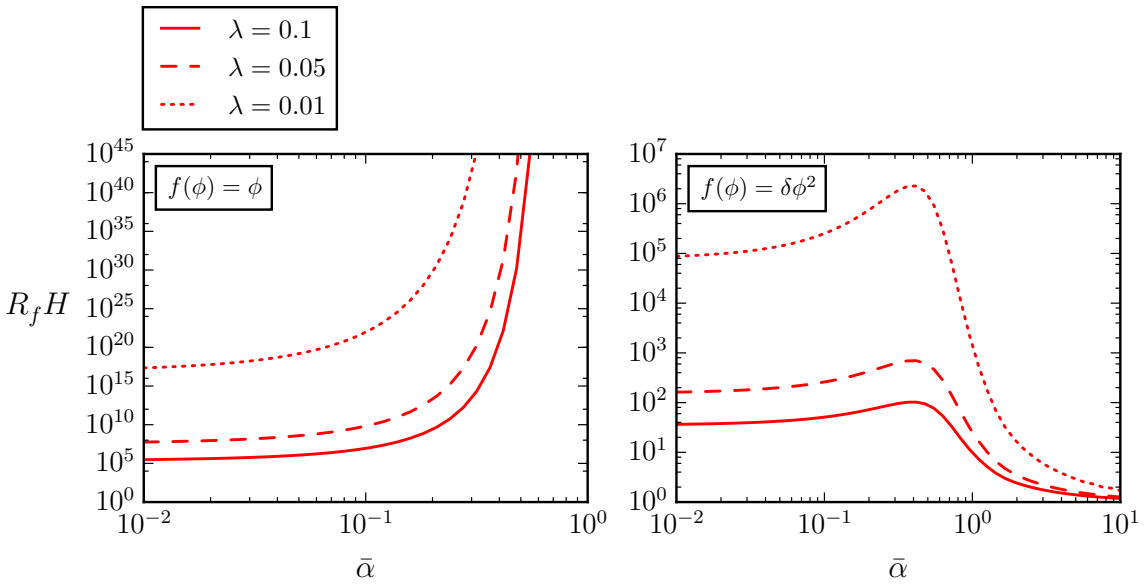

Figure 6. The correlation radii for $f(\phi) = \phi$ and $f(\phi) = \delta\phi^2 \equiv \phi^2 - \langle\phi^2\rangle$ for three values of λ.

5.3 Asymmetric potential

In the asymmetric case discussed in section 4, we can see further examples of these non-trivial hierarchies. When $\bar{\alpha}$ is small, the lowest state $n = 1$ corresponds to perturbative fluctuations around the true vacuum. However, as $\bar{\alpha}$ increases, other states overtake it one by one, as we can see from figure 4.

Figure 5 shows the eigenfunctions for $\bar{\alpha} = 1$ and $\beta = 0.5$, and illustrates that for these parameters the lowest excited state that has significant overlap with the vacuum is $n = 4$. Because of this, this state continues to have the highest spectral coefficient, and therefore it dominates the correlator at short distances. On the other hand, the asymptotic long-distance behaviour is given by the lowest state Λ_1. Because the corresponding spectral coefficient is very small, it only starts to dominate the correlator at extremely long super-horizon distances.

When the potential $V(\phi)$ has two non-degenerate minima separated by a high barrier, the lowest state $n = 1$ is localised in the false vacuum state, and therefore we can interpret it as the contribution from the domains of false vacuum which are occasionally formed. The eigenvalue Λ_1 represents the size of these domains, and the spectral coefficient is suppressed because of their rarity.

However, in the example shown in figure 5 this behaviour occurs even though the potential $V(\phi)$ has only one minimum and there is therefore no false vacuum state (see figure 1). In that case the lowest state $n = 1$ corresponds to excursions of the field into high field values far away from the minimum.

As in the asymmetric case, it is possible that Λ_1 is so small that the false vacuum domains are larger than $1/H_0$. Then, because the true and false vacuum have different physical properties, the observables we would measure would depend on the vacuum we are in. This would not affect the eigenvalues in the spectral expansion (2.6), but the spectral coefficients f_n would have to be computed using the false vacuum ground state ψ_1 rather than the true ground state ψ_0.

JCAP03(2020)049

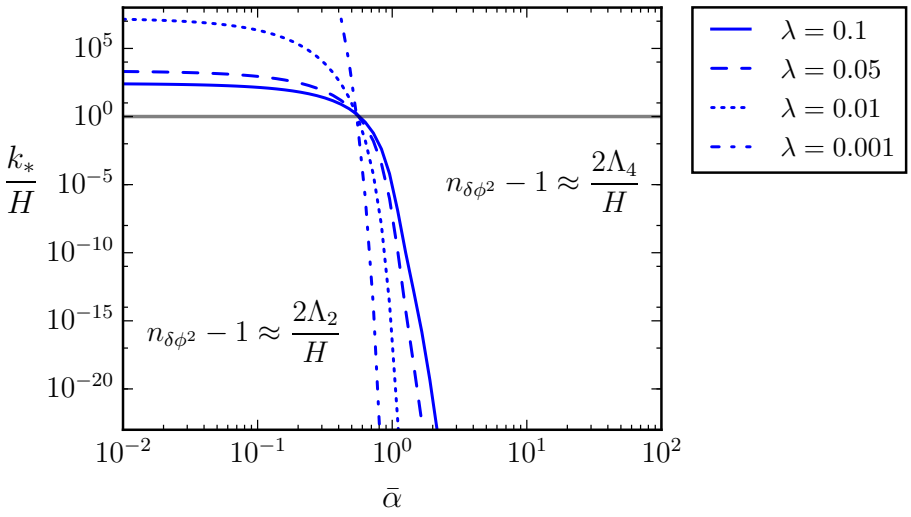

Figure 7. The wavenumber k_* at which the $\mathcal{P}^{(2)}_{\delta\phi^2}(k)$ term starts dominating the power spectrum (5.5) over $\mathcal{P}^{(4)}_{\delta\phi^2}(k)$. Above the gray line the distances are sub-horizon and hence not amendable to a stochastic treatment.

5.4 Power spectrum

For cosmological observations, the power spectrum is often a more relevant quantity than the coordinate-space correlator. Therefore it is useful to calculate the power spectrum by taking the Fourier transform of (2.6)

$$\mathcal{P}_f(k) = \sum_n \frac{2}{\pi} f_n^2 \,\Gamma\left(2 - 2\frac{\Lambda_n}{H}\right) \sin\left(\frac{\Lambda_n \pi}{H}\right) \left(\frac{k}{H}\right)^{2\Lambda_n/H} \equiv \sum_{n=1} \mathcal{P}_f^{(n)}(k)\,, \tag{5.5}$$

where k is the physical momentum.

Assuming that a single $n = d$ term dominates the expansion, the spectral index n_f can then be written in a simple form

$$n_f - 1 \equiv \frac{\ln \mathcal{P}_f(k)}{\ln k} \approx \frac{\ln \mathcal{P}_f^{(d)}(k)}{\ln k} = \frac{2\Lambda_d}{H}. \tag{5.6}$$

When there are non-trivial hierarchies between the spectral coefficients, the spectral index n_f can be different on different scales. As an example, consider the power spectrum of $\delta\phi^2 \equiv \phi^2 - \langle\phi^2\rangle$ in the symmetric case. At asymptotically small wave number k, the spectral index is given by the lowest state $n = 2$, but because its spectral coefficient is very small, the higher state $n = 4$ dominates at higher k. Comparing these two terms, we can straightforwardly solve for the wavenumber k_* at which they cross as

$$\frac{\mathcal{P}^{(2)}_{\delta\phi^2}(k_*)}{\mathcal{P}^{(4)}_{\delta\phi^2}(k_*)} = 1 \quad \Leftrightarrow \quad \frac{k_*}{H} = \left\{ \frac{\left[\langle(\phi^2)_2\rangle\right]^2 \Gamma\left(2 - 2\frac{\Lambda_2}{H}\right) \sin\left(\frac{\Lambda_2\pi}{H}\right)}{\left[\langle(\phi^2)_4\rangle\right]^2 \Gamma\left(2 - 2\frac{\Lambda_4}{H}\right) \sin\left(\frac{\Lambda_4\pi}{H}\right)} \right\}^{\frac{H}{2(\Lambda_4 - \Lambda_2)}}, \tag{5.7}$$

which is plotted in figure 7. When $\bar{\alpha} \lesssim 1$, $k_*/H \gtrsim 1$, and therefore the first term $n = 2$ dominates on all scales and the spectral index is therefore constant to a good approximation.

JCAP03(2020)049

However, when $\bar{\alpha} \gtrsim 1$, we can see that k_*/H rapidly becomes very small, which means the crossover happens at scales that were massively superhorizon during inflation. What this shows is that the scale at which the spectral index changes can for some parameter values occur at scales that are visible in the cosmic microwave background or other cosmological observations, possibly providing an important observational signature of early Universe models involving decoupled spectator scalars.

6 Conclusions

In this work we have studied spectator scalar fields in de Sitter space with a potential of the double-well form (1.1) by means of the stochastic spectral expansion [16]. The terms in the expansion are determined by eigenvalues and eigenfunctions which we solve numerically. This work is a continuation of ref. [59] where only potentials with manifest $\mathbb{Z}_2$ symmetry and a single minimum were considered. Our calculations show that also asymmetric potentials with multiple minima can be efficiently studied with simple numerical methods to high precision, implying the technique to be rather powerful and suitable for a large class of potentials. In this vein we note two interesting possibilities that are yet unexplored: models with more than one scalar and/or potentials with periodic boundary conditions such as for the axion.

The double-well potential has unsurprisingly a much richer structure in terms of eigenfunctions and -values than the quartic or quadratic cases. In particular, the spectrum has states that are not localised near the minimum of the potential and which are therefore not visible in perturbation theory. In most cases these non-perturbative states dominate the correlation function especially at long distances. The spectral coefficients of the terms can also be very different, which can lead to non-trivial behaviour such as a change of the spectral index at very long distances. If this happens at cosmologically relevant scales, it can be observable. Interestingly, this behaviour persists even when the potential has only one minimum. In the symmetric case, the behaviour of odd quantities (such as the field) is also very different from the behaviour of even quantities (such as energy density). Together, these effects demonstrate that the naive intuition based perturbation theory is, in general, not applicable.

Based on our analysis we conclude that spectator fields with a double-well potential have many possibly observable and currently unexplored cosmological consequences.

Acknowledgments

We thank Jacopo Fumagalli, Gabriel Moreau, Julien Serreau and Sébastien Renaux-Petel for illuminating discussions. AR is supported by the U.K. Science and Technology Facilities Council grant ST/P000762/1 and an IPPP Associateship. This project has received funding from the European Union's Horizon 2020 research and innovation programme under the Marie Skłodowska-Curie grant agreement No. 786564.

A Eigenfunctions and -values

Figures 8–12 show the lowest eigenfunctions and eigenvalues for some representative choices for $\bar{\alpha}$ and β. The various values for $\bar{\alpha}$ and β have been specifically chosen as to in include as many qualitatively different cases as possible. The blue dashed lines indicate the locations of the minima. Note that in the non-degenerate case with $\beta \neq 0$ the global minimum is located left of the origin.

JCAP03(2020)049

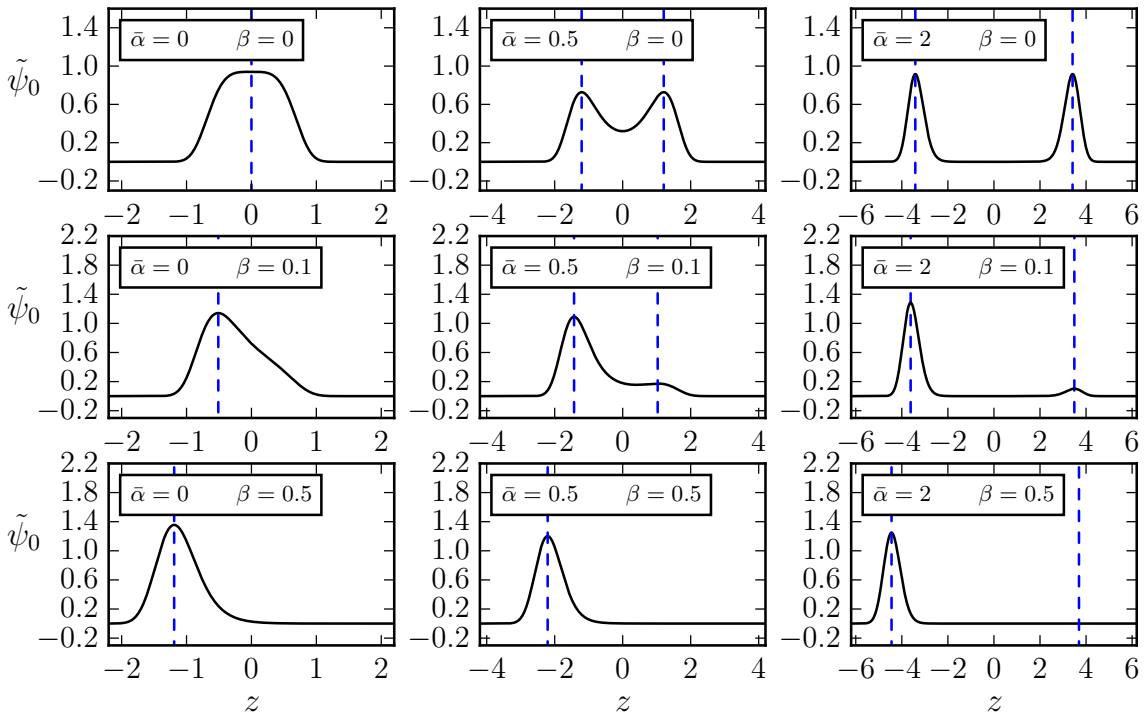

Figure 8. The dimensionless $n = 0$ eigenfunctions from eq. (2.9).

JCAP03(2020)049

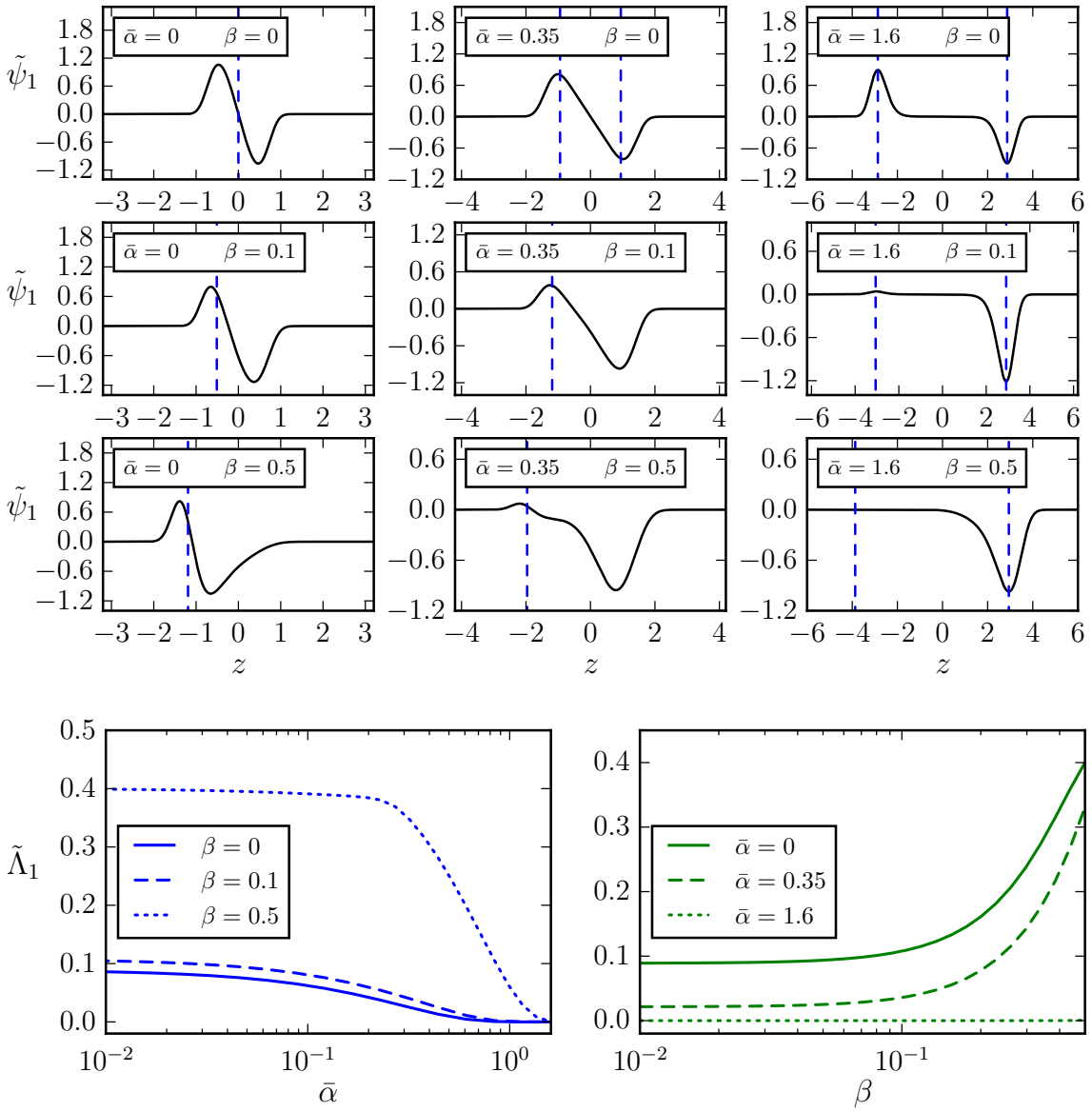

Figure 9. The dimensionless $n = 1$ eigenfunctions and -values from eq. (2.9).

JCAP03(2020)049

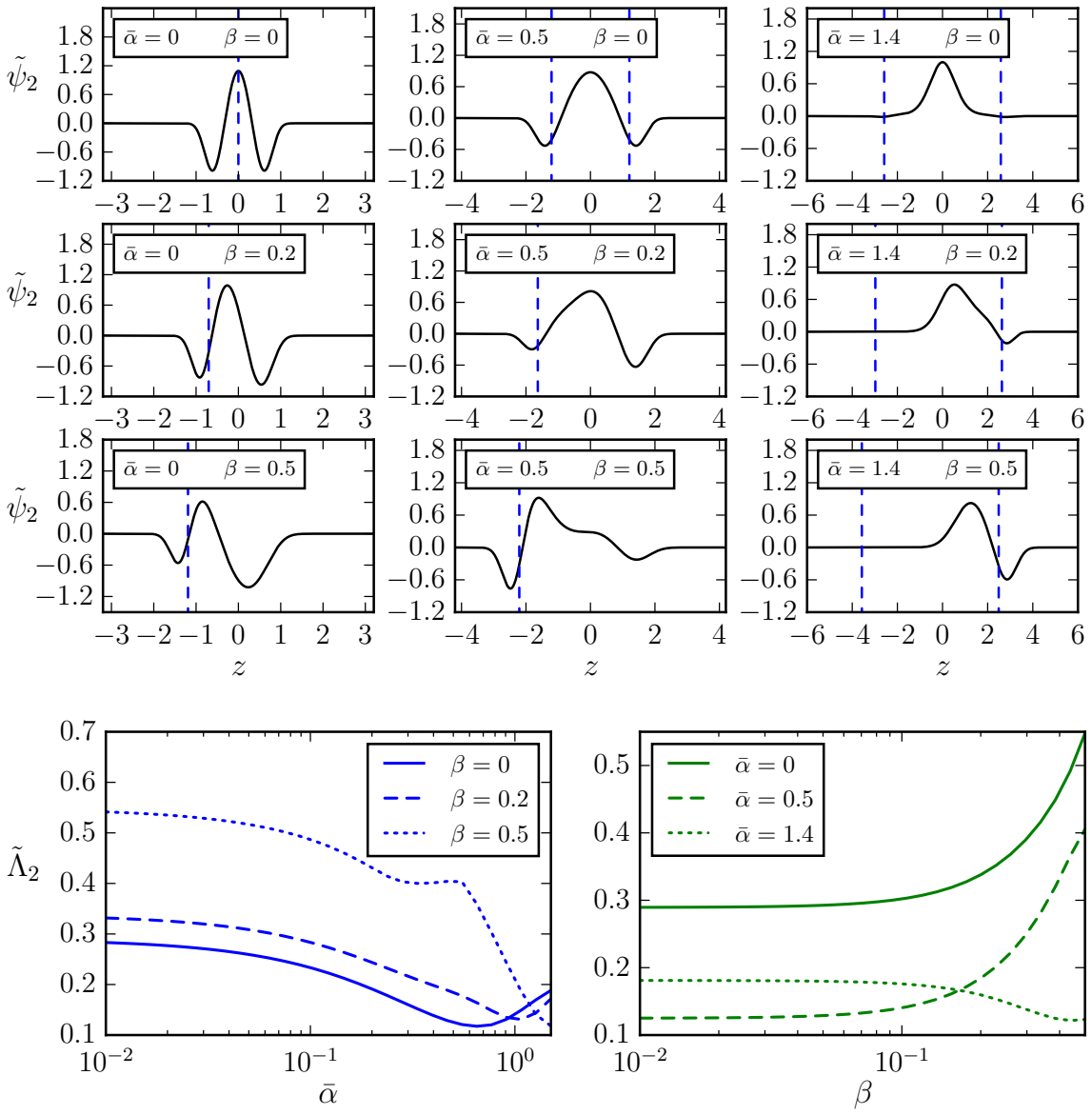

Figure 10. The dimensionless $n = 2$ eigenfunctions and -values from eq. (2.9).

JCAP03(2020)049

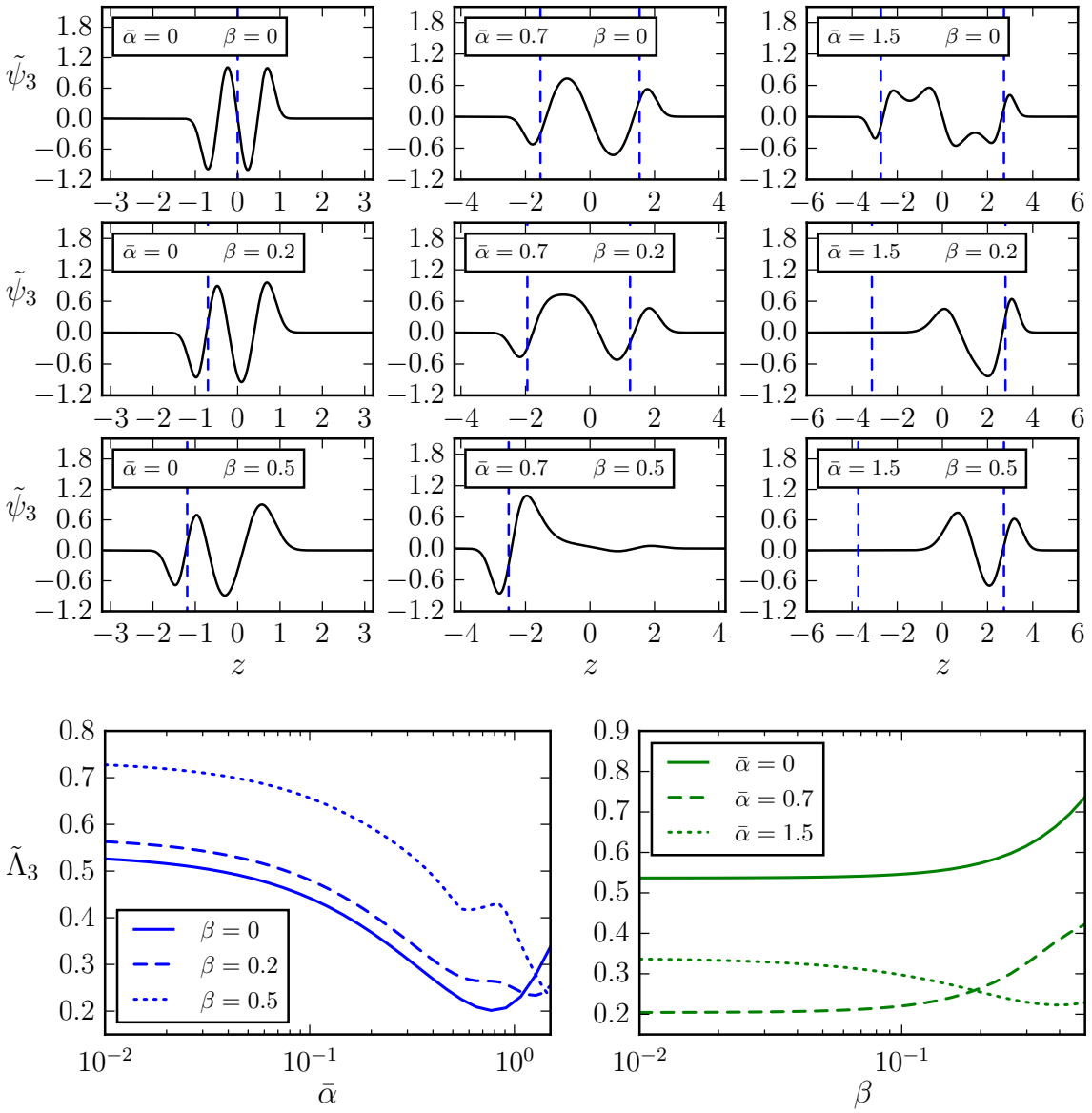

Figure 11. The dimensionless $n = 3$ eigenfunctions and -values from eq. (2.9).

JCAP03(2020)049

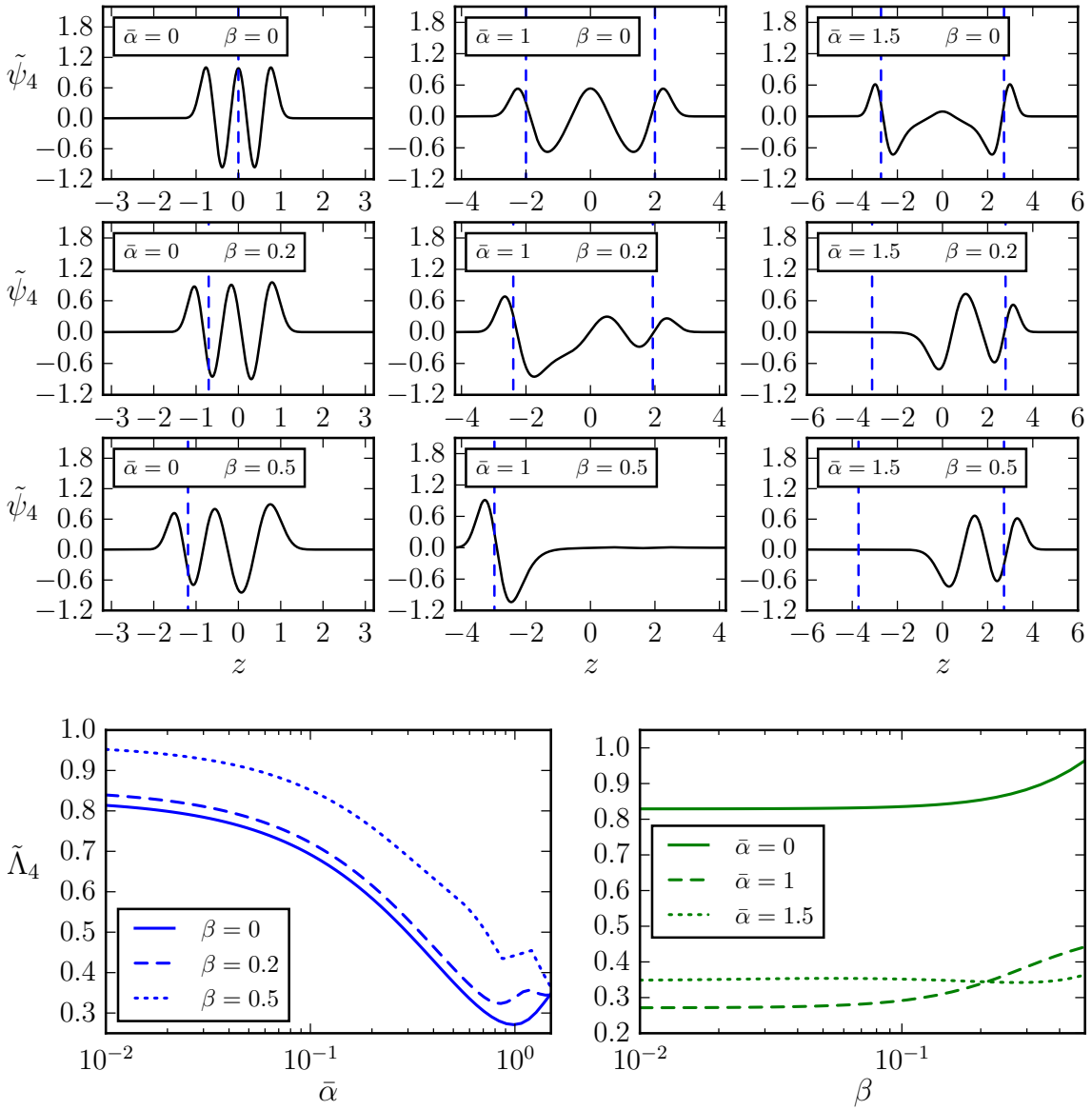

Figure 12. The dimensionless $n = 4$ eigenfunctions and -values from -values from eq. (2.9).

References

[1] N.A. Chernikov and E.A. Tagirov, *Quantum theory of scalar fields in de Sitter space-time*, *Ann. Inst. H. Poincare Phys. Theor.* **A9** (1968) 109.

[2] J.S. Dowker and R. Critchley, *Effective Lagrangian and energy momentum tensor in de Sitter space*, *Phys. Rev.* **D 13** (1976) 3224 [INSPIRE].

[3] T.S. Bunch and P.C.W. Davies, *Quantum field theory in de Sitter space: renormalization by point splitting*, *Proc. Roy. Soc. Lond.* **A 360** (1978) 117 [INSPIRE].

[4] N.D. Birrell and P.C.W. Davies, *Quantum fields in curved space*, Cambridge Monographs on Mathematical Physics, Cambridge Univ. Press, Cambridge, U.K. (1984).

JCAP03(2020)049

[5] A.D. Linde, *Scalar field fluctuations in expanding universe and the new inflationary universe scenario*, *Phys. Lett.* **116 B** (1982) 335 [INSPIRE].

[6] B. Allen, *Vacuum states in de Sitter space*, *Phys. Rev.* **D 32** (1985) 3136 [INSPIRE].

[7] B. Allen and A. Folacci, *The massless minimally coupled scalar field in de Sitter space*, *Phys. Rev.* **D 35** (1987) 3771 [INSPIRE].

[8] V. Gorbenko and L. Senatore, $\lambda\phi^4$ *in dS*, arXiv:1911.00022 [INSPIRE].

[9] P.J.E. Peebles and A. Vilenkin, *Noninteracting dark matter*, *Phys. Rev.* **D 60** (1999) 103506 [astro-ph/9904396] [INSPIRE].

[10] W. Hu, R. Barkana and A. Gruzinov, *Cold and fuzzy dark matter*, *Phys. Rev. Lett.* **85** (2000) 1158 [astro-ph/0003365] [INSPIRE].

[11] T. Markkanen, A. Rajantie and T. Tenkanen, *Spectator dark matter*, *Phys. Rev.* **D 98** (2018) 123532 [arXiv:1811.02586] [INSPIRE].

[12] J.R. Espinosa, G.F. Giudice and A. Riotto, *Cosmological implications of the Higgs mass measurement*, *JCAP* **05** (2008) 002 [arXiv:0710.2484] [INSPIRE].

[13] M. Herranen, T. Markkanen, S. Nurmi and A. Rajantie, *Spacetime curvature and the Higgs stability during inflation*, *Phys. Rev. Lett.* **113** (2014) 211102 [arXiv:1407.3141] [INSPIRE].

[14] T. Markkanen, A. Rajantie and S. Stopyra, *Cosmological aspects of Higgs vacuum metastability*, *Front. Astron. Space Sci.* **5** (2018) 40 [arXiv:1809.06923] [INSPIRE].

[15] A.A. Starobinsky, *Stochastic de Sitter (inflationary) stage in the early universe*, *Lect. Notes Phys.* **246** (1986) 107 [INSPIRE].

[16] A.A. Starobinsky and J. Yokoyama, *Equilibrium state of a selfinteracting scalar field in the de Sitter background*, *Phys. Rev.* **D 50** (1994) 6357 [astro-ph/9407016] [INSPIRE].

[17] B.L. Hu and D.J. O'Connor, *Symmetry behavior in curved space-time: finite size effect and dimensional reduction*, *Phys. Rev.* **D 36** (1987) 1701 [INSPIRE].

[18] D. Boyanovsky, H.J. de Vega and N.G. Sanchez, *Quantum corrections to slow roll inflation and new scaling of superhorizon fluctuations*, *Nucl. Phys.* **B 747** (2006) 25 [astro-ph/0503669] [INSPIRE].

[19] J. Serreau, *Effective potential for quantum scalar fields on a de Sitter geometry*, *Phys. Rev. Lett.* **107** (2011) 191103 [arXiv:1105.4539] [INSPIRE].

[20] M. Herranen, T. Markkanen and A. Tranberg, *Quantum corrections to scalar field dynamics in a slow-roll space-time*, *JHEP* **05** (2014) 026 [arXiv:1311.5532] [INSPIRE].

[21] F. Gautier and J. Serreau, *Infrared dynamics in de Sitter space from Schwinger-Dyson equations*, *Phys. Lett.* **B 727** (2013) 541 [arXiv:1305.5705] [INSPIRE].

[22] F. Gautier and J. Serreau, *Scalar field correlator in de Sitter space at next-to-leading order in a 1/N expansion*, *Phys. Rev.* **D 92** (2015) 105035 [arXiv:1509.05546] [INSPIRE].

[23] J. Tokuda and T. Tanaka, *Statistical nature of infrared dynamics on de Sitter background*, *JCAP* **02** (2018) 014 [arXiv:1708.01734] [INSPIRE].

[24] T. Arai, *Nonperturbative infrared effects for light scalar fields in de Sitter space*, *Class. Quant. Grav.* **29** (2012) 215014 [arXiv:1111.6754] [INSPIRE].

[25] M. Guilleux and J. Serreau, *Quantum scalar fields in de Sitter space from the nonperturbative renormalization group*, *Phys. Rev.* **D 92** (2015) 084010 [arXiv:1506.06183] [INSPIRE].

[26] T. Prokopec and G. Rigopoulos, *Functional renormalization group for stochastic inflation*, *JCAP* **08** (2018) 013 [arXiv:1710.07333] [INSPIRE].

JCAP03(2020)049

[27] G. Moreau and J. Serreau, *Backreaction of superhorizon scalar field fluctuations on a de Sitter geometry: A renormalization group perspective*, *Phys. Rev.* **D 99** (2019) 025011 [arXiv:1809.03969] [INSPIRE].

[28] G. Moreau and J. Serreau, *Stability of de Sitter spacetime against infrared quantum scalar field fluctuations*, *Phys. Rev. Lett.* **122** (2019) 011302 [arXiv:1808.00338] [INSPIRE].

[29] D. López Nacir, F.D. Mazzitelli and L.G. Trombetta, *To the sphere and back again: de Sitter infrared correlators at NTLO in 1/N*, *JHEP* **08** (2019) 052 [arXiv:1905.03665] [INSPIRE].

[30] G. Rigopoulos, *Thermal Interpretation of Infrared Dynamics in de Sitter*, *JCAP* **07** (2016) 035 [arXiv:1604.04313] [INSPIRE].

[31] J. Tokuda and T. Tanaka, *Can all the infrared secular growth really be understood as increase of classical statistical variance?*, *JCAP* **11** (2018) 022 [arXiv:1806.03262] [INSPIRE].

[32] D. Cruces, C. Germani and T. Prokopec, *Failure of the stochastic approach to inflation beyond slow-roll*, *JCAP* **03** (2019) 048 [arXiv:1807.09057] [INSPIRE].

[33] D. Glavan, T. Prokopec and A.A. Starobinsky, *Stochastic dark energy from inflationary quantum fluctuations*, *Eur. Phys. J.* **C 78** (2018) 371 [arXiv:1710.07824] [INSPIRE].

[34] R.J. Hardwick, V. Vennin, C.T. Byrnes, J. Torrado and D. Wands, *The stochastic spectator*, *JCAP* **10** (2017) 018 [arXiv:1701.06473] [INSPIRE].

[35] V. Vennin and A.A. Starobinsky, *Correlation Functions in Stochastic Inflation*, *Eur. Phys. J.* **C 75** (2015) 413 [arXiv:1506.04732] [INSPIRE].

[36] I. Moss and G. Rigopoulos, *Effective long wavelength scalar dynamics in de Sitter*, *JCAP* **05** (2017) 009 [arXiv:1611.07589] [INSPIRE].

[37] J. Grain and V. Vennin, *Stochastic inflation in phase space: Is slow roll a stochastic attractor?*, *JCAP* **05** (2017) 045 [arXiv:1703.00447] [INSPIRE].

[38] H. Firouzjahi, A. Nassiri-Rad and M. Noorbala, *Stochastic Ultra Slow Roll Inflation*, *JCAP* **01** (2019) 040 [arXiv:1811.02175] [INSPIRE].

[39] L. Pinol, S. Renaux-Petel and Y. Tada, *Inflationary stochastic anomalies*, *Class. Quant. Grav.* **36** (2019) 07LT01 [arXiv:1806.10126] [INSPIRE].

[40] R.J. Hardwick, T. Markkanen and S. Nurmi, *Renormalisation group improvement in the stochastic formalism*, *JCAP* **09** (2019) 023 [arXiv:1904.11373] [INSPIRE].

[41] J. Fumagalli, S. Renaux-Petel and J.W. Ronayne, *Higgs vacuum (in)stability during inflation: the dangerous relevance of de Sitter departure and Planck-suppressed operators*, *JHEP* **02** (2020) 142 [arXiv:1910.13430] [INSPIRE].

[42] M. Jain and M.P. Hertzberg, *Eternal Inflation and Reheating in the Presence of the Standard Model Higgs*, arXiv:1910.04664 [INSPIRE].

[43] G. Moreau and J. Serreau, *Unequal Time Correlators of Stochastic Scalar Fields in de Sitter Space*, *Phys. Rev.* **D 101** (2020) 045015 [arXiv:1912.05358] [INSPIRE].

[44] C. Pattison, V. Vennin, H. Assadullahi and D. Wands, *Stochastic inflation beyond slow roll*, *JCAP* **07** (2019) 031 [arXiv:1905.06300] [INSPIRE].

[45] T. Prokopec and G. Rigopoulos, $\Delta\mathcal{N}$ *and the stochastic conveyor belt of Ultra Slow-Roll*, arXiv:1910.08487 [INSPIRE].

[46] G. Franciolini, G.F. Giudice, D. Racco and A. Riotto, *Implications of the detection of primordial gravitational waves for the Standard Model*, *JCAP* **05** (2019) 022 [arXiv:1811.08118] [INSPIRE].

[47] N.C. Tsamis and R.P. Woodard, *Stochastic quantum gravitational inflation*, *Nucl. Phys.* **B 724** (2005) 295 [gr-qc/0505115] [INSPIRE].

JCAP03(2020)049

[48] T. Prokopec, N.C. Tsamis and R.P. Woodard, *Stochastic Inflationary Scalar Electrodynamics*, *Annals Phys.* **323** (2008) 1324 [arXiv:0707.0847] [INSPIRE].

[49] A. Riotto and M.S. Sloth, *On resumming inflationary perturbations beyond one-loop*, *JCAP* **04** (2008) 030 [arXiv:0801.1845] [INSPIRE].

[50] T. Kunimitsu and J. Yokoyama, *Higgs condensation as an unwanted curvaton*, *Phys. Rev.* **D 86** (2012) 083541 [arXiv:1208.2316] [INSPIRE].

[51] H. Motohashi, T. Suyama and J. Yokoyama, *Consequences of a stochastic approach to the conformal invariance of inflationary correlators*, *Phys. Rev.* **D 86** (2012) 123514 [arXiv:1210.2497] [INSPIRE].

[52] B. Garbrecht, G. Rigopoulos and Y. Zhu, *Infrared correlations in de Sitter space: field theoretic versus stochastic approach*, *Phys. Rev.* **D 89** (2014) 063506 [arXiv:1310.0367] [INSPIRE].

[53] B. Garbrecht, F. Gautier, G. Rigopoulos and Y. Zhu, *Feynman diagrams for stochastic inflation and quantum field theory in de Sitter space*, *Phys. Rev.* **D 91** (2015) 063520 [arXiv:1412.4893] [INSPIRE].

[54] C.P. Burgess, R. Holman, G. Tasinato and M. Williams, *EFT beyond the horizon: stochastic inflation and how primordial quantum fluctuations go classical*, *JHEP* **03** (2015) 090 [arXiv:1408.5002] [INSPIRE].

[55] V.K. Onemli, *Vacuum fluctuations of a scalar field during inflation: quantum versus stochastic analysis*, *Phys. Rev.* **D 91** (2015) 103537 [arXiv:1501.05852] [INSPIRE].

[56] T. Prokopec, *Late time solution for interacting scalar in accelerating spaces*, *JCAP* **11** (2015) 016 [arXiv:1508.07874] [INSPIRE].

[57] G. Cho, C.H. Kim and H. Kitamoto, *Stochastic dynamics of infrared fluctuations in accelerating universe*, in *Proceedings, 2nd LeCosPA symposium: everything about gravity, celebrating the centenary of Einstein's general relativity (LeCosPA2015): Taipei, Taiwan, 14–18 December 2015*, pp. 162–167, (2017), arXiv:1508.07877 [INSPIRE].

[58] H. Kitamoto, *Infrared resummation for derivative interactions in de Sitter space*, *Phys. Rev.* **D 100** (2019) 025020 [arXiv:1811.01830] [INSPIRE].

[59] T. Markkanen, A. Rajantie, S. Stopyra and T. Tenkanen, *Scalar correlation functions in de Sitter space from the stochastic spectral expansion*, *JCAP* **08** (2019) 001 [arXiv:1904.11917] [INSPIRE].

[60] D. Griffiths and D.F. Schroeter, *Introduction to quantum mechanics* (3rd ed.), Cambridge University Press, New York (2018).

JCAP03(2020)049